Chemico-Biological Interactions 418 (2025) 111586

Contents lists available at ScienceDirect

Chemico-Biological Interactions

journal homepage: www.elsevier.com/locate/chembioint

Research paper

Tamoxifen regulates ferroptosis of hepatocytes by targeting SLC1A5 to activate hepatic stellate cells and liver fibrosis

Sha Shi [a], Meiling Zhang [a], Chengkai Zhu [a], Shanhao Zhu [a], Jie Yu [c], Qi Sui [a], Jiaqi Xu [a], Juan Ren [c], Jingnan Zhang [a,d,*], Peng Chen [b,**], Yi Zhang [a,d,***]

[a] School of Pharmaceutical Sciences, Hangzhou Medical College, Hangzhou, Zhejiang, 310012, China
[b] Department of Pharmacy, School of Medicine, Hangzhou City University, 50 Huzhou Rd, Hangzhou, Zhejiang, 310015, China
[c] School of Laboratory Medicine and Bioengineering, Hangzhou Medical College, Hangzhou, Zhejiang, 310012, China
[d] Zhejiang TCM Key Laboratory of Pharmacology and Translational Research of Natural Products, Hangzhou Medical College, China

ARTICLE INFO

Keywords:
Liver fibrosis
Drug-induced liver injury
Tamoxifen
Hepatocyte ferroptosis
Hepatic stellate cells
Solute carrier family 1 member 5

ABSTRACT

Tamoxifen (TAM) is a commonly used drug for breast cancer treatment, mainly inhibiting estrogen receptors to prevent tumor growth. Although TAM has achieved remarkable effects in clinical treatment, recent studies have shown that TAM can cause drug-induced liver injury. However, it's still unclear whether long-term use of TAM can cause liver fibrosis. This study explores whether long-term administration of TAM can cause liver fibrosis and its mechanism. We found that TAM could induce liver injury in mice and significantly up-regulate the expression of activation markers of stellate cells, activating the TGF-β/smad signaling pathway. Additionally, TAM induced an inflammatory response and activated the NF-κB signaling pathway. More importantly, we demonstrated for the first time *in vivo* and *in vitro* that TAM-induced hepatocyte ferroptosis, accompanied by glutathione (GSH) depletion, reactive oxygen species (ROS) accumulation, and intracellular ferrous enrichment, and changes in the expression of ferroptosis-related proteins. Ferroptosis inhibitors such as ferrostatin-1 (Fer-1) and DFO ameliorated ferroptosis in hepatocytes. However, these ferroptotic events did not occur in macrophages and hepatic stellate cells (HSCs). Co-culture experiments showed that TAM-induced hepatocytes could increase expression of liver fibrosis-related proteins in HSCs, but this could be abolished by ferroptosis inhibitors. Bioinformatics analysis suggested TAM may regulate hepatocyte ferroptosis through solute carrier family 1 member 5 (SLC1A5). Downregulation of SLC1A5 could inhibit TAM-induced hepatocyte ferroptosis, thereby alleviating HSCs activation and the increased expression of ECM proteins. Our study suggests that TAM induces hepatocyte ferroptosis through SLC1A5, leading to HSC activation and liver fibrosis.

Abbreviations

		TNF-α	tumor necrosis factor
		IL-6	interleukin 6
HSCs	hepatic stellate cells	IL-1β	interleukin-1β
ECM	extracellular matrix	NF-κB	nuclear factor-κB
DILI	drug-induced liver injury	GPX4	glutathione peroxidase 4
α-SMA	α-smooth muscle actin	SLC7A11	solute carrier family 7 member 11
TAM	Tamoxifen	SLC40A1	solute carrier family 40 member 1
GSH	glutathione	GO	gene ontology

(*continued on next column*)

(*continued*)

ROS	reactive oxygen species	KEGG	Kyoto Encyclopedia of Genes and Genomes
ALT	alanine aminotransferase	Icam1	Intercellular Adhesion Molecule 1
AST	aspartate aminotransferase	mito-DAMPs	mitochondria-derived damage-associated molecular patterns
HYP	hydroxyproline	MASP1	mannan-binding lectin serine protease 1
H&E	hematoxylin-eosin	NLRP3	exosomal miRNAs including miR-222, and NOD-, LRR- and

(*continued on next page*)

* Corresponding author. School of Pharmaceutical Sciences, Hangzhou Medical College, Hangzhou, 310012, China.
** Corresponding author. Department of Pharmacy, School of Medicine, Hangzhou City University, Hangzhou, 310015, China.
*** Corresponding author. School of Pharmaceutical Sciences, Hangzhou Medical College, Hangzhou, 310012, China.
E-mail addresses: 749881429@qq.com (J. Zhang), chenp@zucc.edu.cn (P. Chen), 1020437493@qq.com (Y. Zhang).

https://doi.org/10.1016/j.cbi.2025.111586
Received 8 March 2025; Received in revised form 22 May 2025; Accepted 26 May 2025
Available online 26 May 2025

(*continued*)

Abbreviations		TNF-α	tumor necrosis factor
			pyrin domain-containing protein 3
DEGs	differentially expressed genes	SLC39A14	solute carrier family 39 member 14
FBS	fetal bovine serum	PUFAs	polyunsaturated fatty acids
DMEM	Dulbecco's Modified Eagle's Medium	SLC3A2	solute carrier family 3 member 2
siRNAs	small short interfering RNAs	HMGB1	High Mobility Group Box 1
SLC1A5	solute carrier family 1 member 5	TLR4	Toll-like receptor 4
Fer-1	ferrostatin-1	TCA	tricarboxylic acid
MPO	myeloperoxidase	α-KG	α-ketoglutarate
TGF-β	transforming growth factor-β	RSL3	Ras selective lethal 3
smad	small mother against decapentaplegic		

1. Introduction

Liver fibrosis is a complicated inflammation and fibrosis process resulting from chronic liver injury and is an early stage of liver cirrhosis progression. Cirrhosis is a severe liver disease that is the 10th leading cause of death in the Western world, with a 10-year mortality rate of 34–66 % [1]. It is a risk factor for the development of liver cancer [2,3]. In the process of liver fibrosis, hepatic stellate cells (HSCs) are activated into myofibroblasts, which produce an excessive amount of extracellular matrix (ECM) with highly high collagen content and form scar deposits, leading to liver fibrosis [4,5]. Liver fibrosis can be caused by various factors, such as viral infections, metabolic diseases, alcohol, hepatic toxins, biliary diseases, autoimmune, and drug-induced liver injury (DILI) [6]. Studies indicate that acetaminophen can induce hepatocellular injury, releasing inflammatory mediators and cytokines, activating HSCs to up-regulate the expression of α-smooth muscle actin (α-SMA) and type 1 collagen, and secretes a large amount of collagen and other adhesion proteins, invisible gelatinous structures, and ultimately leads to liver fibrosis [7,8].

DILI is a condition that results from direct injury, immune response injury, or other indirect loss of the liver due to the drug itself or drug metabolites [9]. As the central organ of metabolism, the liver is susceptible to drug toxicity. Symptoms of patients with DILI may range from mild elevations in transaminases, and patients may alleviate symptoms by promptly discontinuing the drug or reducing the dose. But if DILI doesn't get timely treatment, it can cause further development for liver fibrosis and even liver failure [10,11]. Certain anti-tuberculosis drugs [12], non-steroidal anti-inflammatory drugs [13], and antipsychotic drugs [14] may induce DILI. Many clinical studies have shown that methotrexate could cause DILI [15]. Recent studies have found that methotrexate causes oxidative stress through the NF-κB pathway and glutathione (GSH) consumption and activates HSCs, causing liver fibrosis [16,17]. Therefore, DILI and liver-related diseases caused by DILI have become an increasingly severe clinical problem.

Tamoxifen (TAM) is an endocrine therapy drug used in cancer treatment. Its structure is similar to estrogen, which can compete with estradiol for the target organ's estrogen receptor to exert an anti-breast cancer effect. TAM has been widely used as a first-line adjuvant endocrine therapy for the treatment of hormone-dependent breast cancer [18,19]. When given as adjuvant therapy, TAM reduces the risk of breast cancer recurrence and death and provides effective remission in patients with metastatic breast cancer [20,21]. However, hepatotoxicity is a common side effect in breast cancer patients treated with TAM. Some studies have reported that TAM can affect lipid metabolism in the liver, cause mitochondrial dysfunction, and produce excess reactive oxygen species (ROS), causing oxidative damage [22–26]. Nonetheless, whether TAM can cause liver fibrosis is unknown, so this was investigated in the present study.

2. Materials and methods

2.1. Experimental animals

Female C57BL/6 mice aged 6–8 weeks were acquired from Hangzhou Medical College. The University Animal Care and Use Committee approved the animal experimental protocol. Mice were randomly divided into two large groups, including one-month and two-month dosing groups. The vehicle group and TAM (25, 50 mg/kg)-treated groups were set up in the two groups, respectively (n = 3–9). TAM (purity: 99.92 %, purchased from MedChemexpres, USA) was dissolved in a 0.5 % sodium carboxymethyl cellulose solution. The TAM-treated groups were given TAM every day via intragastric administration for 1 month or 2 months.

2.1.1. Sample collection

After the treatment, the mice were weighed after 8 h of fasting and constant water, and blood was extracted by removing the eyeball. The blood was stored in a refrigerator at 4 °C for 1 h and then centrifuged at 4 °C, 860 g/min, and 15 min. The supernatant was taken into a new EP tube and stored at −80 °C for later use. And the liver tissue was removed entirely. The liver tissue was separated, weighed, chilled in liquid nitrogen, and kept at −80 °C for use later.

2.2. Serum levels of alanine aminotransferase (ALT), aspartate aminotransferase (AST), and liver hydroxyproline (HYP)

According to the manufacturer's instructions, serum ALT, AST, and liver HYP levels were assessed using HYP reagent kits (Nanjing Jiancheng, China), AST reagent kits (Nanjing Jiancheng, China), and HYP reagent kits (Nanjing Jiancheng, China).

2.3. Liver histological analysis

For the histological assessment of liver injury, liver tissue specimens were immersed in a 4 % paraformaldehyde solution for 24 h. Following fixation, the tissues were sliced into 4-μm-thick sections and subjected to hematoxylin-eosin (H&E) staining. Additionally, Masson's trichrome and Sirius red staining techniques were employed to identify and visualize the presence of collagen within the liver tissues of the mice.

2.4. Immunofluorescence staining for α-SMA

For the immunofluorescence detection of α-SMA, liver tissue sections were incubated with primary α-SMA antibodies in a humidified chamber at 4 °C for an extended period overnight. Subsequently, the sections were exposed to FITC (fluorescein isothiocyanate)-labeled secondary antibodies for 1 h. The fluorescent images were captured using an inverted IX81 microscope (Olympus, Tokyo, Japan).

2.5. Immunohistochemical staining with F4/80

3 % hydrogen peroxide and 3 % bovine serum albumin were used to block liver sections for 1 h. The liver sections were treated with diluted F4/80 antibody and incubated at 4 °C for 16–20 h after being rinsed once with PBS. Following three rinses with PBS, the tissue sections were incubated with a secondary antibody raised in goat and specific for rabbit antibodies, and this incubation was conducted at ambient temperature for 1 h. Hematoxylin was used to stain the nuclei of the tissue slices after they had been cleaned with PBS three times and rinsed with a 3,3-diaminobenzidine tetrahydrochloride chromogenic solution. Following a thorough dehydration process using 75 % and 85 % alcohol for 6 min each, the liver sections were cleaned and rinsed with

anhydrous ethanol and n-butanol until they were clear.

2.6. Transcriptome sequencing and bioinformatics analysis

Liver tissues were separated from the control and TAM 50 mg/kg groups of mice that received a two-month TAM treatment. Following the manufacturer's operating instructions, TRIzol was used to isolate and purify the RNA from the whole sample. Hangzhou Lianchuan Biotechnology (Hangzhou, China) performed mRNA sequencing on the extracted RNA samples. Following the generation of mRNA profiles, fragments per kilobase per million exon models were calculated using StringTie to predict the expression levels of all transcripts. The threshold criteria for identifying differentially expressed genes (DEGs) were fold change≥2 (absolute value of log2FC≥1) and q value < 0.05 (adjusted p-value). Bioinformatic analysis was performed using the OmicStudio tools at https://www.omicstudio.cn/tool.

2.7. Cell culture

HepaRG cells were grown in RPMI 1640 medium containing 10 % fetal bovine serum (FBS), 1 % penicillin G (100 U/mL), and streptomycin (100 μg/mL) in a 37 °C, 5 % CO_2 incubator. LX-2 cells were grown in DMEM (Dulbecco's Modified Eagle's Medium) containing 10 % FBS, 1 % penicillin G (100 U/mL), and streptomycin (100 μg/mL) in a 37 °C, 5 % CO_2 incubator. RAW264.7 cells were grown in DMEM medium containing 10 % FBS in a 37 °C, 5 % CO_2 incubator.

2.8. RNA interference analyses

Small short interfering RNAs (siRNAs) targeting the solute carrier family 1 member 5 (SLC1A5) gene sequence (5′-UGACCUCAACUACAUGGUUTT-3′) were designed and synthesized by GenePharma (China). HepaRG cells were inoculated into 6-well plates and added siRNAs, cultured in RPMI 1640 medium supplemented with 10 % FBS in a 5 % CO_2 incubator at 37 °C for 24 h. Then, a Western blot was used to determine the efficiency of gene knockout.

2.9. Cell viability assay

HepaRG cells were seeded in 96-well plates at a concentration of 3000 cells per well, while LX-2 and RAW264.7 cells were plated at a lower density of 1000 cells per well. Subsequently, the cells were exposed to TAM at 15 and 30 μM concentrations for 24 h. The assessment of cell viability in these plates was performed using the CCK-8 assay kit (APE × BIO Technologies, USA). During the assay, the CCK-8 reagent was incubated with the cells at a temperature of 37 °C for 1 h. Next, a multifunctional enzyme marker (SpectraMax iD5, Molecular Devices, China) measured the 96-well plates at a wavelength of 405 nm.

2.10. Co-culture experiments of HSCs and hepatocytes

HepaRG cells were seeded at 20,000 per well in transwell permeable support membrane inserts (0.4 μm, Corning, USA). Cells were cultured in 24-well plates (Corning, USA) with 400 μl medium added to both transwell and 24-well plates, and then incubated with ferrostatin-1 (Fer-1) for 6 h, siRNAs for 24 h or untreaded, followed by TAM (30 μM) for 24 h. Meanwhile, LX-2 cells were seeded in 24-well plates (Corning, USA) at a density of 30,000 cells per well and starved for 24 h with serum-free DMEM after cell attachment. Then, the medium in HepaRG cells and LX-2 cells was replaced with standard medium, and the transwell containing HepaRG was transferred to the top of LX-2 cells and co-cultured for 24 h. After co-culture was finished, LX-2 cells in 24-well plates were collected for Western blot analysis.

2.11. Myeloperoxidase (MPO) assay

The liver tissue of the groups that were treated with TAM for two months, as well as the control group, was taken. The MPO level in liver tissue was determined using an MPO Kit (Nanjing Jiancheng, China) following the manufacturer's instructions.

2.12. GSH assay

The liver tissue of the groups that were treated with TAM for two months and the control group was clipped. After homogenizing the tissue with normal saline, the mixture was centrifuged for 10 min at 2500 rpm, and the supernatant was collected. The GSH level in liver tissue was determined using a GSH Kit (Nanjing Jiancheng, China), which strictly adhered to the protocol provided by the manufacturer. Similarly, HepaRG cells, LX-2 cells, and RAW264.7 cells were drug-treated and grown as described above, and then the cells were collected. The level of GSH was determined using a GSH Kit (Nanjing Jiancheng, China) following the manufacturer's instructions.

2.13. ROS assay

25 mg of liver tissue was taken, washed with 500 μl pre-cooled PBS, and centrifuged at 500 g at 4 °C for 10 min. Ten times, the pre-cooled PBS homogenate was added and centrifuged at 500 g at 4 °C for 10 min. Take the supernatant in a new tube, discard the precipitation, and centrifuge 10000*g* at 4 °C for 15 min. BCA (ThermoFisher, USA) was measured in the supernatant, precipitated with 500 μl PBS and blown, and centrifuged 10000*g* at 4 °C for 15 min. The supernatant was subsequently removed, and the pellet was resuspended in 150 μl of PBS containing 10 μM of the fluorescent probe DCFH-DA (Beyotime, China). This mixture was then incubated for 1 h. The fluorescence intensity for each sample was quantified using a multifunctional microplate reader, the SpectraMax iD5, a product of Molecular Devices in China.

HepaRG cells, LX-2 cells, and RAW264.7 cells were seeded into 6-well plates and administered according to different experimental protocols when the cell density reached 70 %. Cells were incubated with 1 μM DCFH-DA (Beyotime, China) in DMEM for 20 min at 37 °C. After staining, the cells underwent three successive washes with DMEM to remove the excess probe. Following the washing steps, the cellular structures were promptly imaged. The fluorescence of all samples was observed and recorded using an inverted fluorescence microscope (EVOS M7000, USA).

2.14. Ferrous ion level determination

The ferrous iron levels of liver tissue were measured using the Ferrous Iron Colorimetric Assay Kit (Elabscience, China), which strictly adhered to the protocol provided by the manufacturer. Similarly, HepaRG cells, LX-2 cells, and RAW264.7 cells were seeded into 6-well plates and administered according to different experimental protocols when the cell density reached 70 %. Cells were stained with 1 μM FerroOrange (Dojingo, Japan) in Hoechst 33258 staining solution for 30 min at 37 °C. Finally, the structures were imaged immediately. All the above samples were visualized with a fluorescence-inverted microscope (EVOS M7000, USA).

2.15. Real-time qPCR analysis

Total RNA from liver tissue was isolated using the TRIzol reagent (Accurate Biology, China). The quantity of RNA was ascertained by measuring the optical density at 260 nm. Subsequently, cDNA synthesis was achieved with the PrimeScript RT Master Mix kit (Yeasen, Shanghai, China). Applying SYBR green premix for real-time quantitative PCR (qPCR) was executed using the manufacturer's protocol. The comparative expression levels of the target gene were calculated using the $2^{-\Delta\Delta Ct}$

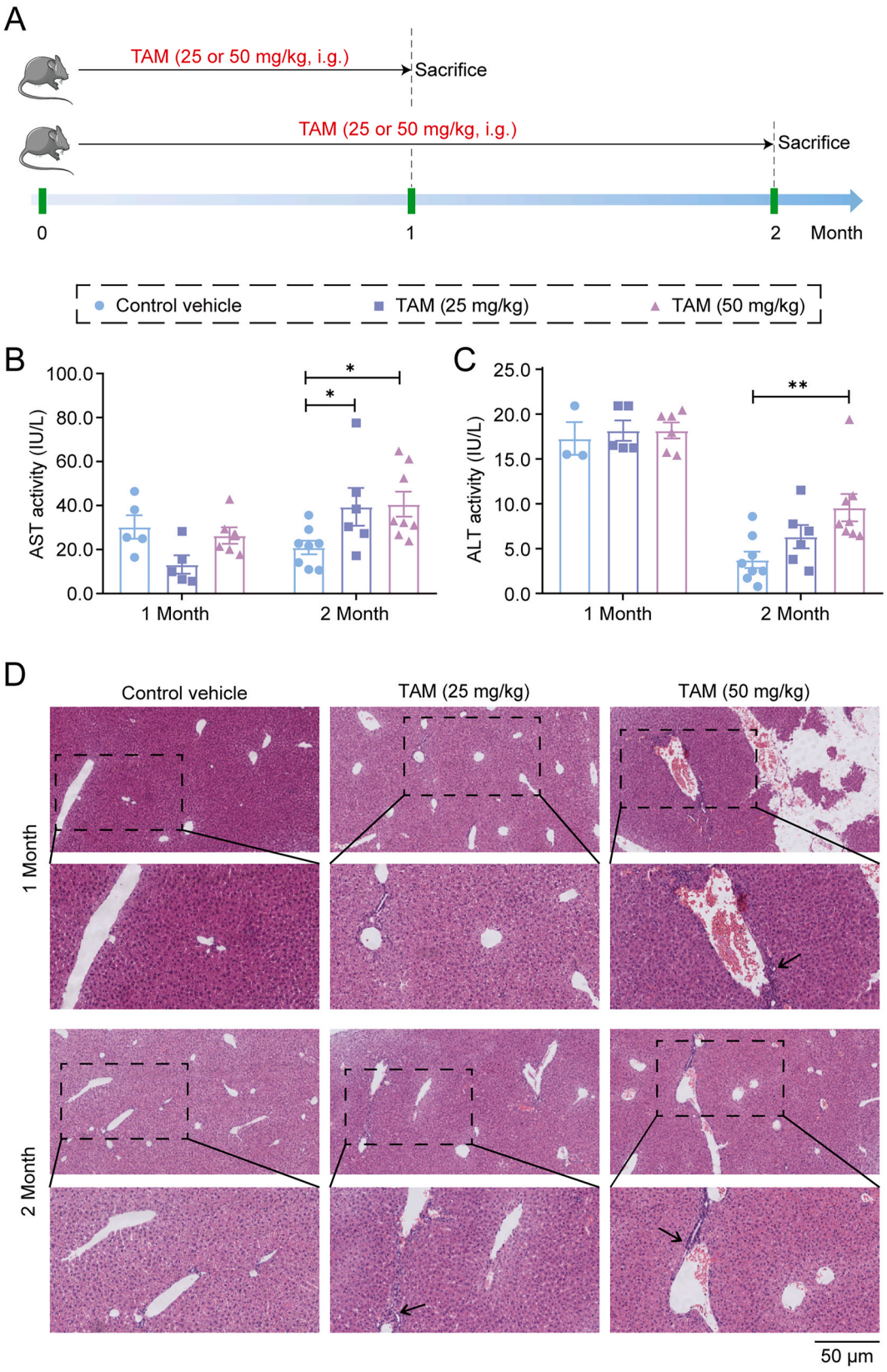

Fig. 1. Serum activities of transaminases and liver histological observation. **(A)** Schematic illustration of the design of animal experiments in mice administration with TAM. **(B)** ALT activity. **(C)** AST activity. Data are expressed as mean ± SEM (n = 3–8). **(D)** Liver H&E staining. Representative images were selected from each experimental group. The hepatic presence of immune cell infiltration is denoted by arrows in the images, with the original magnification set at × 100 for the upper set of images, while the lower images are partial enlargements for a closer view. *$p < 0.05$; **$p < 0.01$.

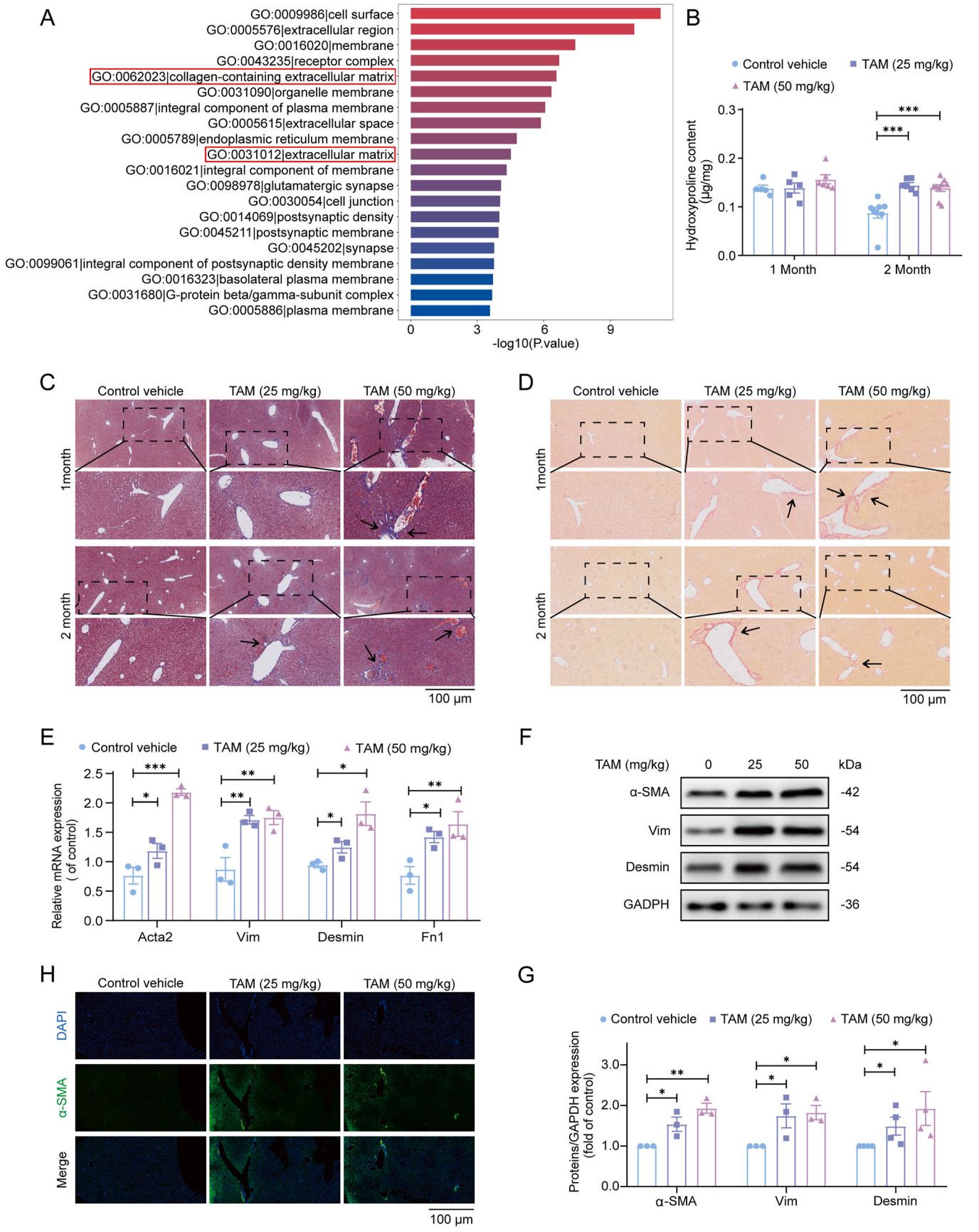

(caption on next page)

Fig. 2. TAM induced liver fibrosis. **(A)** mRNA sequencing analysis of hepatic tissue from control and treated groups after two months of treatment: GO analysis showed the top 20 cellular components involved in the DEGs. **(B)** Hepatic HYP content (n = 5–9). **(C)** Liver sections were stained using Masson's trichrome staining, and representative photographs were selected for each experimental group to illustrate the findings. Collagen fibers are indicated by black arrows within the images, with the upper images displayed at an original magnification of × 200 and the lower images providing a partial enlargement for enhanced detail. **(D)** Liver sections were also subjected to Sirius red staining, with exemplary images selected from each experimental group to highlight the presence of collagen. The upper images are presented at an original magnification of × 200, while the lower images are magnified to examine the collagen deposition closer. After two months of treatment with TAM, **(E)** the mRNA level of liver Acta2 (α-SMA), Vim (vimentin), Desmin (desmin), and Fn1 (fibronectin 1) was assayed by RT-qPCR (n = 3), **(F)** Western blot analyses of liver α-SMA, Vim (Vimentin) and desmin proteins were performed. GAPDH was used as a loading control. **(G)** The results are quantified(n = 3–4), **(H)** Immunofluorescence staining for α-SMA in liver tissues was conducted and captured at an original magnification of × 100. The resulting data were reported as average values accompanied by SEM. *$p < 0.05$; **$p < 0.01$; ***$p < 0.001$. (For interpretation of the references to color in this figure legend, the reader is referred to the Web version of this article.)

method, with the results normalized to a control group. The primer sequences employed in this study are detailed in Supplementary Table 1.

2.16. Western blot analysis

Mouse liver and cellular protein extracts were obtained using the RIPA lysis buffer from Beyotime, China. The lysates were centrifuged at 12,000 g for 5 min at a cool temperature of 4 °C, after which the supernatant, rich in proteins, was meticulously harvested. The protein content of each sample was quantified and normalized to ensure consistency. For protein separation, SDS-PAGE was employed, and the resolved proteins were then transferred to a PVDF membrane. The membranes were pre-treated with a 5 % bovine serum albumin (BSA) solution for 1 h to prevent non-specific protein interactions. The primary antibody binding occurred overnight at 4 °C, succeeded by a 1-h incubation with the corresponding secondary antibodies at ambient temperature. The protein bands on the membranes were detected using an enhanced chemiluminescence assay kit.

Protein lysates from mouse liver and cellular tissues were prepared using the RIPA buffer (Beyotime, China). The proteins ' supernatant was carefully collected after centrifugation at 12,000 g for 5 min at 4 °C. Protein concentrations were measured and adjusted to a uniform level across all samples. Subsequently, the proteins were resolved via SDS-PAGE and transferred onto a PVDF membrane. The membranes, now bearing the proteins, were incubated with a 5 % BSA solution for 1 h to block non-specific binding sites. They were then incubated with the primary antibodies at 4 °C throughout the night, followed by a 1-h incubation with the appropriate secondary antibodies at room temperature. Finally, the proteins on the membranes were visualized using an enhanced chemiluminescence detection kit.

Primary antibodies used in this experiment were GAPDH (HuaBio, China), α-SMA, transforming growth factor-β (TGF-β), small mother against decapentaplegic (smad)2/3, *p*-smad2/3, tumor necrosis factor (TNF-α), interleukin 6 (IL-6), interleukin-1 beta (IL-1β) (Cell Signaling Technology, USA), desmin, vimentin, nuclear factor-κB (NF-κB) p65, phospho–NF–κB p65, lamin B, glutathione peroxidase 4 (GPX4), solute carrier family 7 member 11 (SLC7A11), solute carrier family 40 member 1 (Ferroportin, SLC40A1), transferrin, transferrin receptor, SLC1A5 (ABclonal, China). The secondary antibodies utilized in the procedure were peroxidase-tagged anti-rabbit IgG and peroxidase-tagged anti-mouse IgG (HuaBio, China).

2.17. Statistical analysis

Data is presented as mean ± SEM. Significant differences were found using one-way ANOVA and LSD post hoc tests, with $P < 0.05$ indicating statistical significance.

3. Results

3.1. TAM induced liver injury in mice

The standard oral dose of TAM for breast cancer treatment is 20 mg/day (approximately 0.3 mg/kg for a 60 kg adult). Based on interspecies dose conversion using body surface area, the equivalent dose in mice is approximately 3.7 mg/kg [27]. However, the activity of CYP2D6 enzyme (the primary metabolizing enzyme of TAM) in mice is higher than that in humans, which may lead to faster drug clearance and require higher doses to maintain effective concentrations [28]. Therefore, higher than human equivalent doses of TAM are commonly employed in murine models to assess hepatotoxicity. Meanwhile, doses ranging from 20 to 200 mg/kg have frequently been used to simulate chronic exposure or investigate toxicological mechanisms in previous animal studies [29–32]. Taking these factors into comprehensive consideration, as the experimental doses for this study. As shown in Fig. 1A, we used 38 female mice and divided them into a solvent control group, TAM (25 mg/kg) and TAM (50 mg/kg) groups. Take liver tissue and serum from each group of mice for relevant liver injury indicators detection after administering TAM (25, 50 mg/kg) for 1 month and 2 months, respectively. Consistent with previous studies, we found that after one month of treatment with TAM, there were no apparent differences in ALT and AST serum levels in mice. Still, these levels significantly increased after two months of treatment with TAM (Fig. 1B and C). Liver H&E staining showed no significant pathological changes in the livers of mice treated with TAM at a concentration of 25 mg/kg for one month (Fig. 1D). However, liver infiltration of immune cells and hepatocyte swelling occurred in mice treated with TAM at a concentration of 50 mg/kg for one month and 25 and 50 mg/kg for two months (Fig. 1D). Therefore, our results suggest that long-term administration of TAM to mice can induce liver damage.

3.2. TAM induced liver fibrosis in mice

In our quest to elucidate the underlying mechanisms of TAM-induced hepatic alterations in mice, we conducted an mRNA sequencing study. This analysis was performed on liver tissues harvested from mice in both the control cohort and those administered TAM at 50 mg/kg, as pronounced liver injury was observed in the TAM-treated mice over two months. Upon comparison of the TAM-exposed group with the control group, we identified 2337 genes exhibiting significant differential expression, comprising 1996 genes that were up-regulated and 341 that were downregulated. Gene ontology (GO) analysis indicated that the ECM in the liver of mice significantly increased after treatment, especially the collagen-containing ECM, which suggests that long-term administration of TAM to mice will lead to collagen deposition in the liver (Fig. 2A). Hence, we detected the HYP content in mice's liver, which is regarded as a gold standard marker for liver fibrosis [33]. The results showed the HYP content significantly increased after two months of TAM administration compared with the control group (Fig. 2B). Next, we evaluated the degree of liver fibrosis in mice through Masson's trichrome staining and Sirius red staining. As shown in Fig. 2C and D, there was no evident collagen deposition in the vehicle control group. At the same time, TAM (50 mg/kg) After 1 and 2 months, it was found that the liver tissue was separated by fibrotic collagen, and the collagen connective tissue proliferated significantly. In the context of ongoing liver damage, HSCs undergo a transformation characterized by activation and metamorphosis into myofibroblast-like entities, either directly as HSC/myofibroblasts or indirectly through differentiation from HSCs to

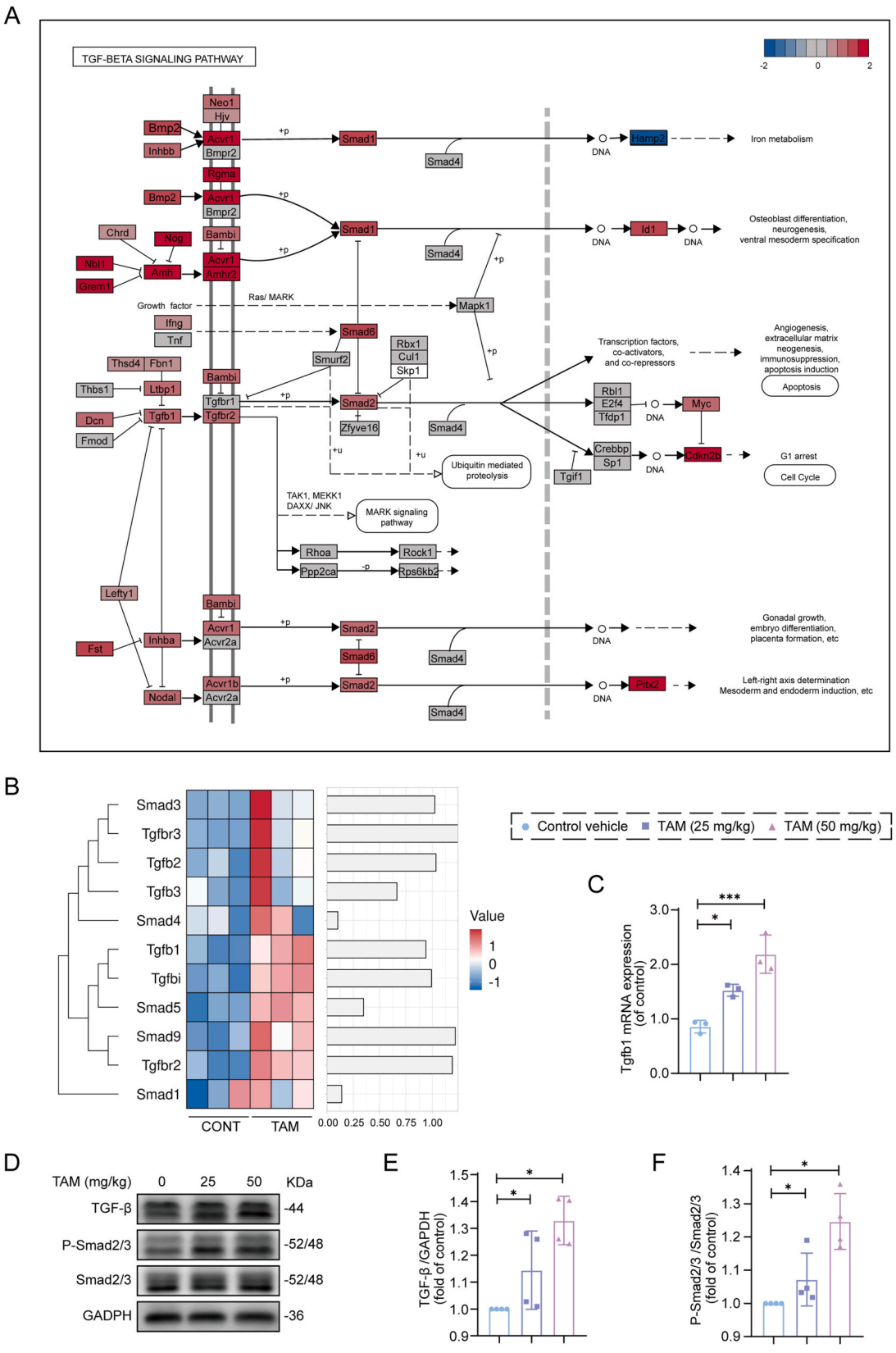

Fig. 3. TAM induced TGF-β/smad *in vivo*. **(A)** The KEGG mapper colored the TGF-β pathway; the red represents up-regulated gene expression, and the blue represents down-regulated gene expression. **(B)** Heatmap mainly shows expression levels of 11 DEGs in the TGF smad pathway. After two months of treatment with TAM, **(C)** the mRNA level of liver TGF-β (Tgfb1) was assayed by RT-qPCR (n = 3), **(D)** Western blot analyses of liver TGF-β and phosphorylated smad2/3 (*p*-smad2/3) proteins were performed, **(E, F)** the results are quantified(n = 3–4). Data were expressed as means ± SEM. *p < 0.05; ***p < 0.001. (For interpretation of the references to color in this figure legend, the reader is referred to the Web version of this article.)

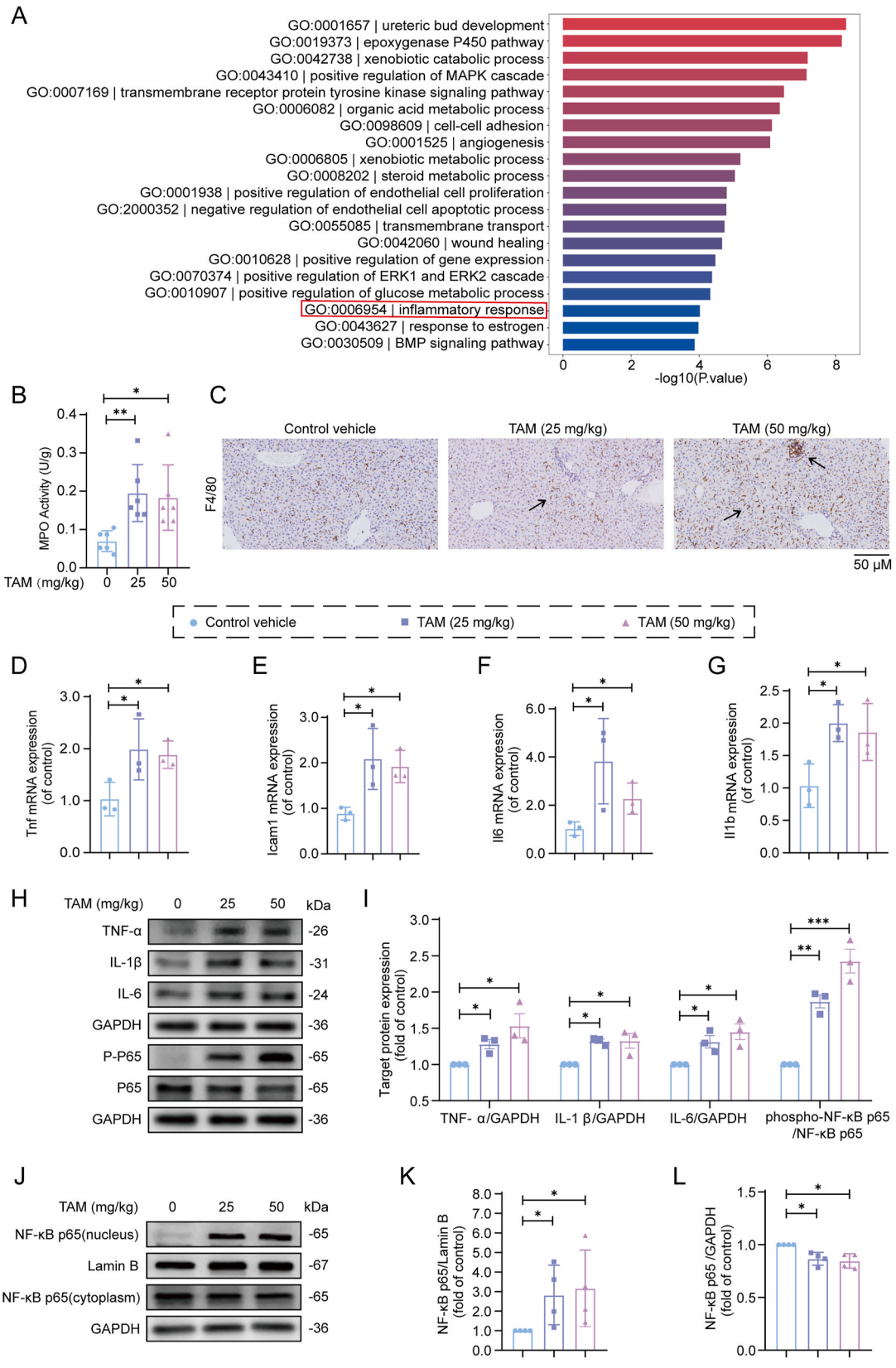

Fig. 4. TAM included inflammation *in vivo*. **(A)** GO analysis showed the top 20 biological progress involved in DEGs. **(B)** Liver MPO content in mice (n = 6). **(C)** Liver F4/80 Immunohistochemical staining (original magnification × 100). **(D–G)** The mRNA level of liver Tnf (TNF-α), Icam1, Il6 (IL-6), and Il1b (IL-1β) was assayed by RT-qPCR (n = 3). **(H)** Western blot analyses of liver TNF-α, IL-1β, IL-6, and hosphor–NF–κB p65 proteins were performed (n = 3), and **(I)** the results were quantified. **(J)** Western blot analyses of liver tissue nucleus and cytoplasmic NF-κB p65 proteins were performed, and GAPDH was used as a loading control. **(K–L)** The results are quantified (n = 3). Data were expressed as means ± SEM. $^{*}p < 0.05$; $^{**}p < 0.01$; $^{***}p < 0.001$.

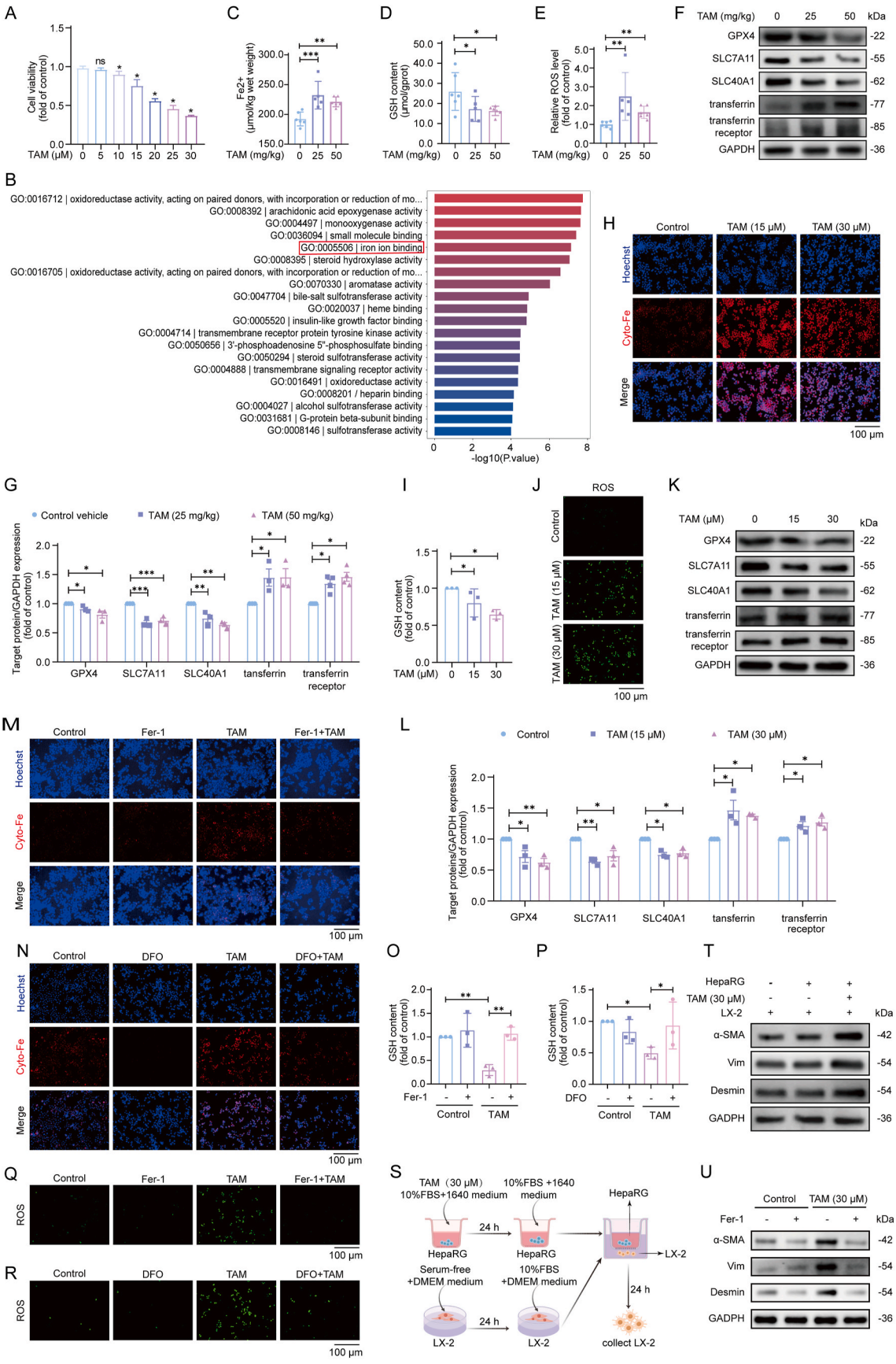

(caption on next page)

Fig. 5. TAM stimulates HSC activation by inducing ferroptosis of hepatocytes. **(A)** Cell viability of HepaRG cells with different concentrations of TAM for 24 h was detected by CCK-8. **(B)** GO analysis showed the top 20 molecular functions involved in DEGs. Liver **(C)** Fe^{2+}, **(D)** GSH content, and **(E)** relative ROS level in mice (n = 5–6). **(F)** Western blot analyses of liver GPX4 SLC7A11, SLC40A1, transferrin, and transferrin receptor proteins were performed, and GAPDH was used as a loading control. (G) The results are quantified (n = 3). **(H)** The intracellular ferrous ion level in HepaRG cell (orange). Nuclei are stained by DAPI (blue). **(I)** The cellular GSH content in HepaRG cell (n = 3). **(J)** The ROS level in HepaRG cell. The samples were observed with a fluorescence-inverted microscope. All samples as described **(H, J)** were observed with a fluorescence inverted microscope. **(K)** Western blot analyses of GPX4 SLC7A11, SLC40A1, transferrin, and transferrin receptor proteins in HepaRG cells were performed, and GAPDH was used as a loading control. **(L)** The results are quantified(n = 3–4). HepaRG cells were exposed to Fer-1(1 μM), DFO (100 μM), or/TAM (30 μM) for 24 h. **(M)** and **(N)** The intracellular ferrous ion level in HepaRG cell (orange). Nuclei are stained by DAPI (blue). **(O)** and **(P)** The cellular GSH content in HepaRG cells (n = 3). **(Q)** and **(R)** The ROS level in HepaRG cell. Observations of the samples were made using an inverted fluorescence microscope, as was the case for all the specimens mentioned **(M, N, Q, R)**. **(S)** The co-culture was established: HepaRG cells were cultured with TAM (30 μM) in a transwell for 24 h, and LX-2 cells were seeded in 24-well plates with serum-free DMEM. After 24 h, the medium in HepaRG cells and LX-2 cells was replaced with normal medium, and the transwell was transferred to 24-well plates with LX-2 cells. 24 h later, LX-2 cells were collected for further testing. **(T)** Western blot analyses of α-SMA, Vim (vimentin), and desmin proteins in LX-2 cells were performed, and GAPDH was used as a loading control. (U) HepaRG cells pretreated with Fer-1 (1 μM) for 6 h were cultured with TAM (30 μM) for 24 h and then co-cultured with starved LX-2 cells for 24 h. LX-2 cells were collected and Western blot analyses of α-SMA, Vim (vimentin), and desmin proteins in LX-2 cells were performed, and GAPDH was used as a loading control. Data were expressed as means ± SEM. $*p < 0.05$; $**p < 0.01$; $***p < 0.001$; ns not significant. (For interpretation of the references to color in this figure legend, the reader is referred to the Web version of this article.)

myofibroblasts. This process is marked by an enhanced production of ECM constituents, predominantly the fibrillar form of collagen. The specific markers of positive HSC/MFs include α-SMA, vimentin, desmin, fibronectin, etc [34,35]. We also found that the mRNA expression of α-SMA, vimentin, desmin, and fibronectin 1 in the liver of mice increased to varying degrees after two months of TAM administration compared with the control group (Fig. 2E). The protein expressions of α-SMA, vimentin, and desmin were also significantly increased in comparison with the control group (Fig. 2F and G). In addition, liver α-SMA immunofluorescence staining showed that TAM administration for two months significantly increased the number of α-SMA-positive cells in mice (Fig. 2H). Together, the data indicate that long-term administration of TAM in mice induces liver fibrosis.

3.3. TAM induced TGF-β/smad in vivo

TGF-β is a well-known profibrotic cytokine. When an injury occurs, TGF-β secretion is increased in the fibrotic microenvironment, and smad2/3 is activated through TGF-β receptor 1/2 [36,37]. Subsequently, phosphorylated smad2/3 enters the nucleus and initiates the expression of ECM by directly targeting downstream genes [36]. The Kyoto Encyclopedia of Genes and Genomes (KEGG) mapper was used to color in targets in the TGF-β pathway (Fig. 3A), and the heatmap showed 11 genes differentially expressed in the TGF-β/smad pathway (Fig. 3B). Bioinformatics results showed that TAM activated TGF-β/smad signaling in mice liver compared with controls. Compared with the control group, the mRNA levels of TGF-β in the livers of mice treated with TAM for two months increased (Fig. 3C), and the protein expression of TGF-β and phosphorylated smad2/3 significantly increased (Fig. 3D–F). In conclusion, TAM may induce liver fibrosis by regulating the TGF-β/smad signaling axis.

3.4. TAM included inflammation in vivo

Based on GO analysis, it was found that TAM-induced liver fibrosis may be related to the induction of inflammatory response (Fig. 4A). To determine this, we examined the granulocyte marker MPO and the macrophage marker F4/80 to check if TAM could affect the degree of neutrophil infiltration/macrophage. We found that MPO activity increased after TAM administration for two months (Fig. 4B). Liver F4/80 Immunohistochemical staining showed abundant expression compared to the control section (Fig. 4C). We also detected the mRNA levels of different proinflammatory mediators in mice liver tissue using RT-qPCR, including TNF-α, Intercellular Adhesion Molecule 1 (Icam1), IL-6, andIL-1β. We found that TAM induced a significant increase in the transcriptional levels of these mediators in the liver (Fig. 4D–G). Additionally, we detected the protein levels of TNF-α, IL-1β, and IL-6 in mice liver tissue using Western blot and found that the proinflammatory mediators significantly increased in the liver (Fig. 4H and I).

To further explore the mechanism of TAM-induced liver inflammation, we detected the phosphorylation level of the NF-κB p65. The NF-κB family of inducible transcription factors represents a family that regulates multiple proinflammatory molecules, including interleukin and TNF-α [38,39]. The NF-κB p65, which harbors transcriptional activation domains, has been extensively investigated [38]. The results showed a significant increase in the level of phospho–NF–κB p65 protein in the liver of mice after TAM administration for two months, compared with controls (Fig. 4H and I). The nuclear translocation of NF-κB p65 plays a crucial role in activating various proinflammatory cytokines, as it serves as a transcriptional regulator for these cytokines. There was also a notable elevation in the level of NF-κB p65 protein within the nucleus, accompanied by a substantial decrease in its cytoplasm (Fig. 4J–L). These findings suggest a potential association between TAM-induced inflammatory response and activation of the NF-κB signaling pathway.

3.5. TAM stimulates HSC activation by inducing ferroptosis of hepatocytes

Our study showed that long-term administration of TAM to mice can cause liver fibrosis. Next, we explored the specific mechanism by which TAM induces liver fibrosis in mice. The HepaRG cell line represents a human bipotent progenitor cell line that can differentiate into cells that resemble hepatic tubules and hepatocytes. These cells exhibit traits and behaviors akin to those of mature hepatocytes and serve as a precious substitute for primary hepatocytes *in vitro* culture settings. The HepaRG cell line is advantageous for drug assessment and metabolism research due to its expression and functionality of a broad array of detoxification enzymes [40]. Consequently, we subjected HepaRG cells to various concentrations of TAM for 24 h. We observed that cell viability was adversely affected by TAM in a concentration-dependent fashion *in vitro* (Fig. 5A). GO analysis revealed that the DEGs were predominantly linked to the binding of iron ions, suggesting the potential occurrence of ferroptosis in the livers of mice following TAM treatment (Fig. 5B). After administration of TAM for two months, the content of ferrous ion in liver tissue was significantly increased, the level of GSH was decreased considerably, and ROS was significantly increased (Fig. 5C–E). The expression of ferroptotic proteins was also changed significantly in the liver of these mice. As shown in Fig. 5F and G, compared with the control group, the protein expressions of GPX4, SLC7A11, and SLC40A1 significantly decreased, and the protein expressions of transferrin and transferrin receptor significantly increased. Together, these findings suggest that ferroptosis may have occurred in the mice liver of mice after TAM administration. Further experiments showed that the levels of intracellular ferrous ions and ROS were significantly higher compared with the controls in the HepaRG cells with TAM for 24 h, while the level of GSH was lower (Fig. 5H–J). The expressions of ferroptotic proteins

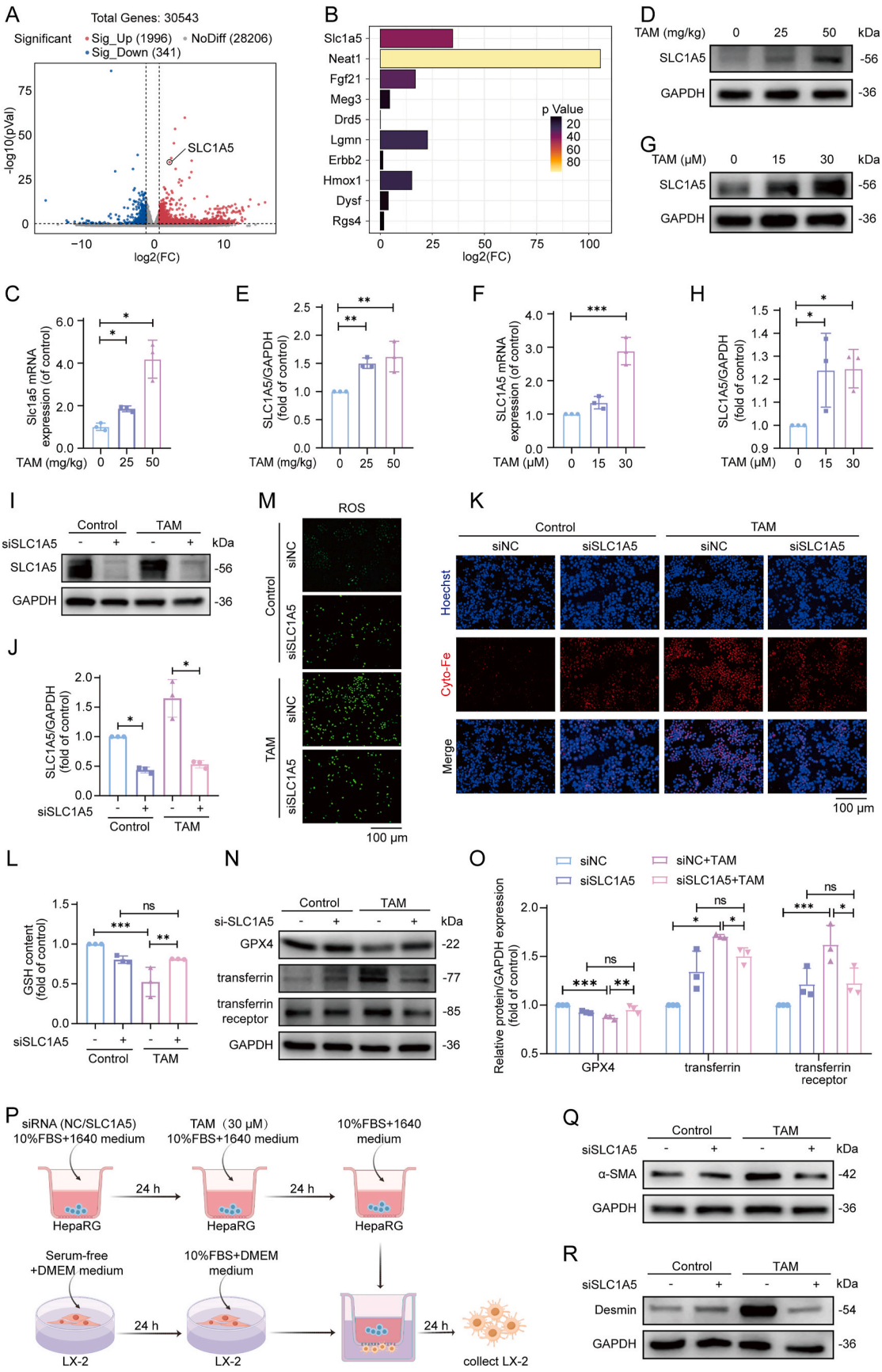

(caption on next page)

Fig. 6. SLC1A5 is involved in the induced fibrotic effect of TAM. **(A)** The volcano map of differential transcriptomic analysis was treated with 50 mg/kg TAM for two months in mice. Transcript variations are categorized as follows: non-significant alterations are marked in grey, significant increases in expression are indicated in red, and significant decreases are denoted in blue. **(B)** Gene enrichment analysis of DEGs related to ferroptosis between control mice and mice treated with 50 mg/kg TAM. After two months of treatment with TAM, **(C)** the mRNA level of liver SLC1A5 was assayed by RT-qPCR (n = 3), **(D)** Western blot analyses of liver SLC1A5 proteins were performed, **(E)** the results are quantified(n = 3). With the HepaRG cells cultured with TAM for 24 h, **(F)** the mRNA level of SLC1A5 was assayed by RT-qPCR (n = 3), **(G)** Western blot analyses of SLC1A5 proteins were performed, **(H)** the results are quantified(n = 3). Exposure of SLC1A5 siRNA to HepaRG cells for 24 h, with or without TAM (30 μM) treatment for 24 h. **(I)** SLC1A5 protein levels were measured by Western blot, and **(J)** the results were quantified(n = 3). **(K)** The intracellular ferrous iron level in HepaRG cell (orange). Nuclei are stained by DAPI (blue). **(L)** The cellular GSH content in HepaRG cell (n = 3). **(M)** The ROS level in HepaRG cell. Observations of the samples were made using an inverted fluorescence microscope, as was the case for all the specimens mentioned **(K, M)**. **(N)** Western blot analyses of GPX4, transferrin, and transferrin receptor proteins in HepaRG cells were performed, and GAPDH was used as a loading control. **(O)** The results are quantified(n = 3). Data were expressed as means ± SEM. $^{*}p < 0.05$; $^{**}p < 0.01$; $^{***}p < 0.001$. **(P)** The co-culture was established as follows: HepaRG cells were exposed to SLC1A5 siRNA for 24 h, cultured in TAM (30 μM) for another 24 h, and then co-cultured with LX-2 cells starved for 24 h to collect LX-2 cells for further testing. Western blot analyses of **(Q)** α-SMA and **(R)** desmin proteins in LX-2 cells were performed, and GAPDH was used as a loading control. (For interpretation of the references to color in this figure legend, the reader is referred to the Web version of this article.)

were also changed significantly with the downregulation of GPX4, SLC7A11, and SLC40A1 and the upregulation of transferrin and transferrin receptor (Fig. 5K–L).

In addition to hepatocytes that comprise most of the liver tissue, the liver also has HSCs activated when the liver is injured, and essential immune cells—macrophages [41]. Therefore, HepaRG, LX-2, and RAW 264.7 (mouse macrophage cell line) cells were cultured with TAM for 24 h, respectively. The results showed that TAM had no significant effect on the viability of LX-2 and RAW 264.7 cells, unlike HepaRG cells (Fig. S1A). Levels of intracellular ferrous ion (Fig. S1B) and ROS content (Fig. S1D) were elevated by TAM in HepaRG cells, while GSH content (Fig. S1C) decreased. However, when exposed to LX-2 and RAW 264.7 cells to TAM, neither showed the ferroptotic events (Fig. S1B–D). To further confirm that TAM can induce hepatocytes ferroptosis, we used two ferroptosis inhibitors in the following experiment. We then exposed HepaRG cells to two ferroptosis inhibitors, Fer-1 and DFO. Interestingly, Fer-1 and DFO could abolish the TAM-induced downregulation of GSH and the upregulation of intracellular ferrous ions and ROS (Fig. 5M–R). The data suggest that TAM induces hepatocyte ferroptosis without directly affecting HSCs and macrophages.

HSC activation stands as a pivotal moment in the progression of liver fibrosis. The LX-2 cell line, a model of HSCs, arises through spontaneous immortalization and is maintained in culture under low serum conditions. This cell line exhibits the2 expression of characteristic markers of stellate cells, including α-SMA, vimentin, and glial fibrillary acidic protein, alongside crucial receptors implicated in liver fibrosis such as platelet-derived growth factor receptor beta, oncostatin M receptor beta, and discoidin domain receptor 2. Microarray analysis showed that LX-2 had a high degree of similarity (98.7 %) in gene expression to primary HSCs, including various neuronal genes [42]. Therefore, LX-2 cells are often used as a disease cell in liver fibrosis research. To investigate whether TAM-induced hepatocyte ferroptosis would affect the activation of HSCs, we co-cultured HepaRG cells exposed to TAM with LX-2 cells starved for 24 h in a serum-free medium (Fig. 5S). Compared to co-culture with normal hepatocytes, the co-culture of TAM-treated hepatocytes with LX-2 resulted in a significant upregulation of liver fibrosis marker proteins, including α-SMA, vimentin, and desmin, in the LX-2 cells (Fig. 5T). Additionally, when comparing LX-2 cells co-cultured with normal hepatocytes to those cultured in isolation, there were no significant differences in the expression levels of the liver fibrosis markers α-SMA, vimentin, and desmin (Fig. 5T). To further verify the role of TAM-induced hepatocyte ferroptosis in stimulating hepatic stellate cell activation, we first pretreated HepaRG cells with the ferroptosis inhibitor Fer-1 for 6 h, then added TAM for 24 h, and then co-cultured them with LX-2 cells that had been starved for 24 h in serum-free medium. The expression of liver fibrosis-related proteins in LX-2 cells was detected and it was found that Fer-1 could reverse the up-regulation of α-SMA, vimentin and desmin in LX-2 cells caused by TAM-induced ferroptosis of HepaRG cells, while it had no significant effect on the expression of α-SMA, vimentin and desmin in LX-2 cells co-cultured with HepaRG cells treated with Fer-1 alone (Fig. 5U). To summarize, the findings indicate that TAM could potentially trigger ferroptosis in hepatocytes and concurrently promote the activation of HSCs, which may lead to liver fibrosis.

3.6. *SLC1A5 is involved in the induced fibrotic effect of TAM*

Our previous studies found that TAM *in vitro* can induce hepatocyte ferroptosis, stimulating HSC activation. To understand how TAM causes hepatocytes ferroptosis, we analyzed transcriptome sequencing data and identified ten up-regulated genes related to ferroptosis. SLC1A5 was the most significant (Fig. 6A–B). Additional experiments showed that SLC1A5 levels were significantly increased in both liver tissue and HepaRG cells treated with TAM (Fig. 6C–H). Using specific siRNA to knock down SLC1A5 expression in HepaRG cells (Fig. 6I and J), we found that depletion of SLC1A5 alleviated TAM-induced downregulation of GSH, and the upregulation of intracellular ferrous ion and ROS (Fig. 6K–M). Additionally, the knockdown of SLC1A5 restored the reduced GPX4 protein level and increased transferrin and transferrin receptor protein levels in TAM-treated HepaRG cells (Fig. 6N and O). Finally, co-culturing SLC1A5-silenced HepaRG cells with LX-2 cells showed that silencing SLC1A5 attenuated the activation of HSCs induced by HepaRG cells (Fig. 6P–R). Based on the above results, we prove that SLC1A5 is vital in TAM-induced hepatocyte ferroptosis, stimulating HSC activation.

4. Discussion

In this study, we found that long-term administration of TAM can induce ferroptosis in hepatocytes, leading to sustained activation of HSCs, which in turn causes liver damage and liver fibrosis. Bioinformatic analysis indicates that TAM may regulate hepatocyte ferroptosis by targeting SLC1A5. Therefore, SLC1A5 may be a target for treating TAM-induced liver fibrosis.

Hepatocytes account for 70 %–80 % of liver tissue and are the main component of the liver. Injury and death to hepatocytes are important initial events in all liver disease etiologies [43–45]. Hepatocellular injury is the central mechanism of inflammation and disease progression in various acute and chronic liver diseases, such as liver fibrosis [46]. When liver damage occurs, hepatocytes are damaged. Their gene expression changes, producing a series of factors, such as mitochondria-derived damage-associated molecular patterns (mito--DAMPs), mannan-binding lectin serine protease 1 (MASP1), exosomal miRNAs including miR-222, and NOD-, LRR- and pyrin domain-containing protein 3 (NLRP3) inflammasome proteins, which directly or indirectly promotes HSCs activation and aggravates the development of liver fibrosis [47–51]. Ferroptosis is a newly discovered method of programmed cell death significantly different from other types of programmed death processes at the morphological, biochemical, and genetic levels [52]. Ferroptosis is characterized by intracellular lipid ROS and iron metabolism disorders [53]. With extensive research and exploration on ferroptosis, some scholars have discovered that the

occurrence of ferroptosis in hepatocytes is related to liver damage and even liver fibrosis [43,44,54,55]. A recent study has shown that fibroblast growth factor 21 is a new ferroptosis inhibitor, which inhibits ferroptosis by targeting heme oxygenase 1 and nuclear factor erythroid 2-related factor 2, thereby resisting ferroptosis-induced hepatocyte mitochondrial damage, liver damage, and fibrosis [44]. Another study found that treating hepatocyte-specific transferrin knockout mice with the ferroptosis inhibitor Fer-1 effectively rescues liver fibrosis induced by a high-iron diet or carbon tetrachloride administration. Moreover, the hepatocyte-specific deletion of the metal transporter Solute Carrier Family 39 Member 14 (SLC39A14) significantly attenuates iron-overload-induced ferroptosis in these mice [43].

Ferroptosis is usually caused by oxidative damage to polyunsaturated fatty acids (PUFAs) on the cell membrane, forming lipid peroxides [56–58]. The accumulation of these peroxides continues to spread through a chain reaction of free radicals, destroying the integrity of the cell membrane. In this process, the accumulation of ferrous ions plays a key role, which catalyzes lipid peroxidation reactions, thereby promoting the production of free radicals, triggering a chain reaction, and exacerbating the peroxidation of lipids on the cell membrane. In addition, the system x_c^- cystine/glutamate antiporter (a transmembrane protein complex containing subunits SLC7A11 and solute carrier family 3 member 2 (SLC3A2)), an important antioxidant system in the cell, resists oxidative stress by regenerating GSH. However, during ferroptosis, the activity of the system x_c^-, may be inhibited, resulting in a decrease in GSH levels, thereby reducing the cell's defense against oxidative damage. Our study found that TAM induced HepaRG cell death in a concentration-dependent manner *in vitro*. Through GO analysis and DEGs enrichment, we discovered many ferroptosis-related genes, and we speculated that TAM induced ferroptosis in hepatocytes. The administration of TAM resulted in decreased GSH content in the liver of mice and in hepatocytes *in vitro*, accompanied by elevated intracellular ferrous ion levels and increased levels of ROS. The changes in intracellular ferrous ion, GSH, and ROS levels caused by TAM in hepatocytes can be reversed by the ferroptosis inhibitors Fer-1 and DFO. The SLC7A11 gene, encoding the light chain component of the system xc-transporter, is chiefly responsible for its principal transport function and exhibits high specificity for the amino acids cystine and glutamate. By facilitating the uptake of cysteine, which in turn enhances the synthesis of GSH, SLC7A11 is instrumental in curbing the buildup of lipid hydroperoxides, thereby safeguarding cells against ferroptosis [59]. GPX4 is an important antioxidant enzyme that maintains ROS balance and is considered a central inhibitory factor of ferroptosis. Its activity depends on GSH produced after activation of the cystine-glutamate antiporter SLC7A11 [60]. We found TAM reduced GXP4 and SLC7A11 protein levels in mice liver and hepatocytes. SLC40A1 is a vital iron ion transporter responsible for the export of intracellular ferrous ions [60]. Impairment or mutation of SLC40A1 function can lead to the accumulation of iron ions in cells. Transferrin is a metal-binding protein primarily synthesized in the liver. After binding to iron ions, it transfers iron ions from the blood into cells by binding to transferrin receptors on the cell surface [61,62]. This process is essential for maintaining the balance of iron ions inside and outside cells. We found that TAM reduced SLC40A1 protein levels in mice livers and hepatocytes, and increased transferrin and transferrin receptor protein levels, which may increase the accumulation of intracellular iron and ferrous ions, aggravate intracellular lipid peroxidation, and thus promote the development of ferroptosis. In addition, we found that TAM can reduce GSH content and increase intracellular ferrous ion levels and ROS levels in hepatocytes, but has less effect on macrophages and HSCs. Hepatocytes, macrophages, and HSCs are all important components of the liver, but our data suggest that TAMs can induce ferroptosis in hepatocytes, but not macrophages and HSCs.

HSC activation is the central mechanism of liver fibrosis, driving scar formation through excessive synthesis of ECM components such as collagen [63]. Emerging evidence highlights the critical role of hepatocyte ferroptosis in HSC activation [64–66]. Ferroptotic hepatocytes release damage-associated molecular patterns (High Mobility Group Box 1 (HMGB1), ATP), which promote HSC proliferation and ECM secretion via Toll-like receptor 4 (TLR4) and purinergic receptor P2Y14 [65]. In our study, we co-cultured hepatocytes treated with TAM for 24 h or pretreated with ferroptosis inhibitors for 6 h and then treated with TAM for 24 h with quiescent HSCs to investigate whether TAM-induced ferroptosis in hepatocytes would have an effect on the activation of quiescent HSCs. The experimental results showed that after co-culture with HepaRG cells treated with TAM for 24 h, the expression of HSC activation markers α-SMA and vimentin and desmin in LX-2 cells was significantly upregulated. However, pre-incubation of hepatocytes with ferroptosis inhibitors rescued the HSC activation and high expression of ECM induced by TAM-induced hepatocyte ferroptosis. These findings suggest TAM-induced hepatocyte ferroptosis stimulates HSC activation, thereby producing ECM proteins. Moreover, hepatocyte ferroptosis is frequently implicated in the initiation of hepatic inflammation. Recent studies have revealed a bidirectional regulatory relationship between liver inflammation and ferroptosis, which collectively promotes fibrogenesis. Specifically, activation of the NF-κB pathway can directly induce hepatocyte ferroptosis by downregulating GSH, SLC7A11 and GPX4 and enhancing ROS [67,68]. Conversely, hepatocyte ferroptosis triggers the release of inflammatory cytokines TNF-α, IL-6, IL-1β and intercellular signaling molecules (TGF-β), which directly or indirectly activate HSCs, thereby driving liver fibrosis [69,70]. Our study demonstrated that TAM induced liver inflammation by upregulating TNF-α, IL-1β and activating NF-κB signaling pathway, and hepatocyte ferroptosis by upregulating intracellular ferrous ions and ROS levels and downregulating GSH level and SLC7A11 and GPX4 protein expression levels, which subsequently activated HSCs. Based on the above literature supports and the results of this study, we speculate that TAM may promotes hepatocyte ferroptosis, derived inflammatory signals further stimulate HSC activation, ultimately contributing to liver fibrosis. However, the precise molecular bridging mechanisms linking TAM-induced ferroptosis, NF-κB activation and cytokine release, remain to be fully elucidated.

SLC1A5 is a critical amino acid carrier system member, mediating the uptake of neutral amino acids, including glutamine [71]. SLC1A5 acts as a predominant transporter mediating cellular glutamine uptake, playing an essential role in glutamine acquisition for metabolic processes [72]. Glutamine, the most abundant amino acid in the body, serves as a critical nitrogen and carbon source for proliferating cells, orchestrating the biosynthesis of nucleotides, amino acids, hexosamines and the replenishment of tricarboxylic acid (TCA) cycle intermediates [72]. This metabolic integration fundamentally requires efficient cellular glutamine uptake, where SLC1A5 functions as the principal transporter governing this rate-limiting step. However, when cells are treated with ferroptosis inducers such as erastin and (Ras selective lethal 3) RSL3, glutamate produced by glutamine catabolism is broken down and metabolized into α-ketoglutarate (α-KG) through the TCA cycle, resulting in the production of high levels of ROS and oxidizable lipids, leading to cellular ferroptosis [72–74]. Excessive α-KG generated from glutamine catabolism promotes ROS overproduction through electron transport chain hyperactivation [73,74]. SLC1A5 facilitates glutamine uptake, promoting its catabolism into α-ketoglutarate, which induces excessive ROS generation and lipid peroxidation, thereby inducing cellular ferroptosis. Our research results have found that TAM can induce hepatocyte ferroptosis, so we further analyzed the previous mRNA sequencing data and screened out the most significant genes SLC1A5 associated with ferroptosis. Then, we detected the protein expression of SLC1A5 in liver tissue and hepatocytes, and both were elevated. Next, we investigated whether SLC1A5 plays an essential role in TAM-induced hepatocyte ferroptosis. We found that knockdown of SLC1A5 reversed the TAM-induced elevation of intracellular ferrous ion and ROS, as well as the downregulation of GSH, and restore the protein levels of GPX4, transferrin, and transferrin receptor. The above

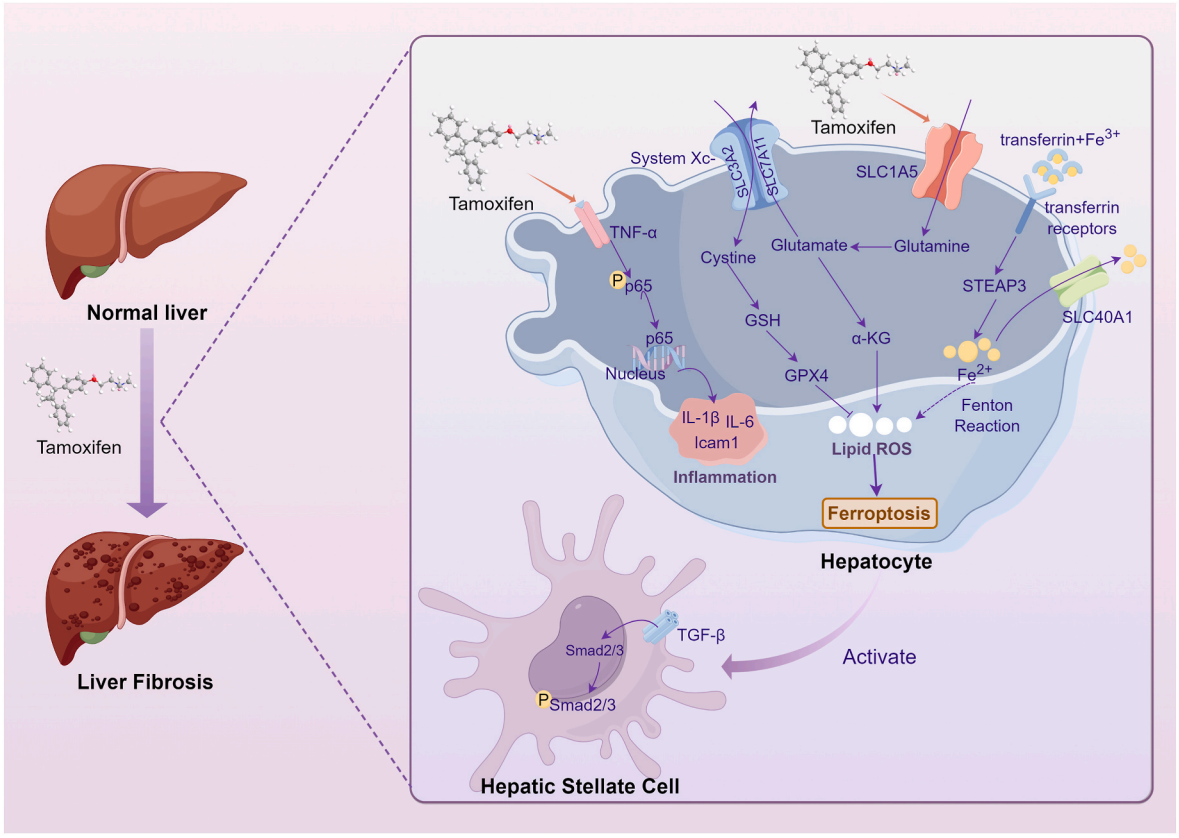

Fig. 7. Schematic illustration of the role and mechanism of tamoxifen in the progression of liver fibrosis. Tamoxifen increases intracellular iron levels in hepatocytes, decreases the content of GSH, and elevates the levels of ROS, thereby inducing ferroptosis in hepatocytes. Following ferroptosis of hepatocytes, HSCs are activated, leading to an upregulation of ECM protein expression. Tamoxifen may induce ferroptosis in hepatocytes by targeting the SLC1A5. Silencing the expression of SLC1A5 can suppress ferroptosis in hepatocytes and inhibit the increase in ECM proteins.

experimental results showed that TAM may induce hepatocyte ferroptosis by targeting SLC1A5. To investigate whether TAM-induced hepatocyte ferroptosis by targeting SLC1A5 induces HSC activation, hepatocytes with knockdown of SLC1A5 were cultured with TAM for 24 h and then co-cultured with quiescent HSC. Detection of liver fibrosis indicators in HSC revealed that low expression of SLC1A5 could reduce the expression of α-SMA and desmin in LX-2 cells caused by TAM-induced ferroptosis of HepaRG cells. The above experimental results prove that TAM may induce hepatocyte ferroptosis by targeting SLC1A5, thereby activating HSCs, promoting the production of ECM proteins, and inducing the occurrence and development of liver fibrosis.

Our findings indicate that TAM can induce liver fibrosis and inflammation, and hepatocyte ferroptosis may lead to HSC activation. The knockdown of SLC1A5 expression abolished ferroptosis in hepatocytes, thereby abolishing HSC activation and increasing the expression of ECM proteins (Fig. 7). This study points out the critical role of hepatocyte ferroptosis in TAM-induced liver fibrosis and provides a new perspective for treating TAM-induced liver fibrosis.

CRediT authorship contribution statement

Sha Shi: Writing – original draft, Data curation. **Meiling Zhang:** Formal analysis. **Chengkai Zhu:** Data curation. **Shanhao Zhu:** Methodology. **Jie Yu:** Resources. **Qi Sui:** Data curation. **Jiaqi Xu:** Data curation. **Juan Ren:** Data curation. **Jingnan Zhang:** Data curation. **Peng Chen:** Writing – review & editing. **Yi Zhang:** Writing – review & editing, Funding acquisition.

Funding

This study was supported by the National Natural Science Foundation of China (82304840 to Y.Z.), Zhejiang Provincial Natural Science Foundation of China under Grant No. LQ23H280021 to Y.Z., Traditional Chinese Medicine Science and Technology Project of Zhejiang Province (2024ZF006 to Y.Z.), Basic Scientific Research Project of Hangzhou Medical College (KYYB202106 to Y.Z.).

Declaration of competing interest

The authors declare that they have no known competing financial interests or personal relationships that could have appeared to influence the work reported in this paper.

Acknowledgment

The main figures were assembled by Figdraw (www.figdraw.com).

Appendix A. Supplementary data

Supplementary data to this article can be found online at https://doi.org/10.1016/j.cbi.2025.111586.

Supplementary material

Supplemental information includes one table. All the other data are available from the authors on request.

Data availability

Data will be made available on request.

References

[1] S. Coulon, F. Heindryckx, A. Geerts, C. Van Steenkiste, I. Colle, H. Van Vlierberghe, Angiogenesis in chronic liver disease and its complications, Liver Int. 31 (2011) 146–162.

[2] G. Cabibbo, M. Maida, C. Genco, M. Antonucci, C. Cammà, Causes of and prevention strategies for hepatocellular carcinoma, Semin. Oncol. 39 (2012) 374–383.

[3] R. Pinyol, S. Torrecilla, H. Wang, C. Montironi, M. Piqué-Gili, M. Torres-Martin, L. Wei-Qiang, C.E. Willoughby, P. Ramadori, C. Andreu-Oller, P. Taik, Y.A. Lee, A. Moeini, J. Peix, S. Faure-Dupuy, T. Riedl, S. Schuehle, C.P. Oliveira, V.A. Alves, P. Boffetta, A. Lachenmayer, S. Roessler, B. Minguez, P. Schirmacher, J.-F. Dufour, S.N. Thung, H.L. Reeves, F.J. Carrilho, C. Chang, A.V. Uzilov, M. Heikenwalder, A. Sanyal, S.L. Friedman, D. Sia, J.M. Llovet, Molecular characterisation of hepatocellular carcinoma in patients with non-alcoholic steatohepatitis, J. Hepatol. 75 (2021) 865–878.

[4] F. Tacke, C. Trautwein, Mechanisms of liver fibrosis resolution, J. Hepatol. 63 (2015) 1038–1039.

[5] T. Kisseleva, D. Brenner, Molecular and cellular mechanisms of liver fibrosis and its regression, Nat. Rev. Gastroenterol. Hepatol. 18 (2021) 151–166.

[6] Q. Pei, Q. Yi, L. Tang, Liver fibrosis resolution: from molecular mechanisms to therapeutic opportunities, Int. J. Mol. Sci. 24 (2023).

[7] T. Radosavljević, D. Mladenović, D. Vucević, R.J. Vukićević, [The role of oxidative/nitrosative stress in pathogenesis of paracetamol-induced toxic hepatitis], Med. Pregl. 63 (2010) 827–832.

[8] J. Tak, Y.S. Kim, T.H. Kim, G.-C. Park, S. Hwang, S.G. Kim, Gα12 overexpression in hepatocytes by ER stress exacerbates acute liver injury via ROCK1-mediated miR-15a and ALOX12 dysregulation, Theranostics 12 (2022) 1570–1588.

[9] M. Garcia-Cortes, M. Robles-Diaz, C. Stephens, A. Ortega-Alonso, M.I. Lucena, R. J. Andrade, Drug induced liver injury: an update, Arch. Toxicol. 94 (2020) 3381–3407.

[10] M. Chayanupatkul, T.D. Schiano, Acute liver failure secondary to drug-induced liver injury, Clin. Liver Dis. 24 (2020) 75–87.

[11] E.S. Björnsson, R.J. Andrade, Long-term sequelae of drug-induced liver injury, J. Hepatol. 76 (2022) 435–445.

[12] Y. Liu, W. Chen, Y. Cen, X. Zhao, Z. Chen, Y. Liang, Z. Huang, X. He, G. Yang, Hepatocyte ferroptosis contributes to anti-tuberculosis drug-induced liver injury: involvement of the HIF-1α/SLC7A11/GPx4 axis, Chem. Biol. Interact. 376 (2023) 110439.

[13] N. Somchit, F. Sanat, E.H. Gan, I.A.W. Shahrin, A. Zuraini, Liver injury induced by the non-steroidal anti-inflammatory drug mefenamic acid, Singapore Med J 45 (2004) 530–532.

[14] N. Todorović Vukotić, J. Đorđević, S. Pejić, N. Đorđević, S.B. Pajović, Antidepressants- and antipsychotics-induced hepatotoxicity, Arch. Toxicol. 95 (2021) 767–789.

[15] V. Di Martino, D.W. Verhoeven, F. Verhoeven, F. Aubin, J. Avouac, L. Vuitton, F. Lioté, T. Thévenot, D. Wendling, Busting the myth of methotrexate chronic hepatotoxicity, Nat. Rev. Rheumatol. 19 (2023).

[16] S. Schmidt, C.J. Messner, C. Gaiser, C. Hämmerli, L. Suter-Dick, Methotrexate-induced liver injury is associated with oxidative stress, impaired mitochondrial respiration, and endoplasmic reticulum stress in vitro, Int. J. Mol. Sci. 23 (2022).

[17] A. Dogra, D. Gupta, S. Bag, I. Ahmed, S. Bhatt, E. Nehra, S. Dhiman, A. Kumar, G. Singh, S.T. Abdullah, P.L. Sangwan, U. Nandi, Glabridin ameliorates methotrexate-induced liver injury via attenuation of oxidative stress, inflammation, and apoptosis, Life Sci. 278 (2021) 119583.

[18] S.R.D. Johnston, New strategies in estrogen receptor-positive breast cancer, Clin. Cancer Res. 16 (2010) 1979–1987.

[19] E.B.C.T.C. Group, Effects of chemotherapy and hormonal therapy for early breast cancer on recurrence and 15-year survival: an overview of the randomised trials, Lancet 365 (2005) 1687–1717.

[20] V.C. Jordan, Tamoxifen: a most unlikely pioneering medicine, Nat. Rev. Drug Discov. 2 (2003) 205–213.

[21] I. Ahmad Shagufta, Tamoxifen a pioneering drug: an update on the therapeutic potential of tamoxifen derivatives, Eur. J. Med. Chem. 143 (2018) 515–531.

[22] Q. Yu, J. Huo, Y. Zhang, K. Liu, Y. Cai, T. Xiang, Z. Jiang, L. Zhang, Tamoxifen-induced hepatotoxicity via lipid accumulation and inflammation in zebrafish, Chemosphere 239 (2020) 124705.

[23] W.-B. Zhou, X.-X. Zhang, Y. Cai, W. Sun, H. Li, Osthole prevents tamoxifen-induced liver injury in mice, Acta Pharmacol. Sin. 40 (2019) 608–619.

[24] D.H. El-Kashef, A.R. El-Sheakh, Hepatoprotective effect of celecoxib against tamoxifen-induced liver injury via inhibiting ASK-1/JNK pathway in female rats, Life Sci. 231 (2019) 116573.

[25] A.C. Famurewa, C.A. Ekeleme-Egedigwe, E.E. David, C.O. Eleazu, A.M. Folawiyo, N.A. Obasi, Zinc abrogates anticancer drug tamoxifen-induced hepatotoxicity by suppressing redox imbalance, NO/iNOS/NF-κB signaling, and caspase-3-dependent apoptosis in female rats, Toxicol. Mech. Methods 30 (2020) 115–123.

[26] Y.-L. Huang, C. De Gregorio, V. Silva, Á.A. Elorza, P. Léniz, V. Aliaga-Tobar, V. Maracaja-Coutinho, M. Budini, F. Ezquer, M. Ezquer, Administration of secretome derived from human mesenchymal stem cells induces hepatoprotective effects in models of idiosyncratic drug-induced liver injury caused by amiodarone or tamoxifen, Cells 12 (2023).

[27] E.G.o.t.C.P.o.T.f.t.T.o.B. Cancer, Expert Consensus on the Clinical Practice of Taxanes for the Treatment of Breast Cancer], Zhonghua Zhong Liu Za Zhi, vol. 42, 2020, pp. 161–169.

[28] J.M. Hoskins, L.A. Carey, H.L. McLeod, CYP2D6 and tamoxifen: DNA matters in breast cancer, Nat. Rev. Cancer 9 (2009) 576–586.

[29] R. Ye, Q.A. Wang, C. Tao, L. Vishvanath, M. Shao, J.G. McDonald, R.K. Gupta, P. E. Scherer, Impact of tamoxifen on adipocyte lineage tracing: inducer of adipogenesis and prolonged nuclear translocation of Cre recombinase, Mol. Metabol. 4 (2015) 771–778.

[30] M.D. Burkitt, J.M. Williams, T. Townsend, R. Hough, C.A. Duckworth, D. M. Pritchard, Mice lacking NF-κB1 exhibit marked DNA damage responses and more severe gastric pathology in response to intraperitoneal tamoxifen administration, Cell Death Dis. 8 (2017) e2939.

[31] C.M. Lee, L. Zhou, J. Liu, J. Shi, Y. Geng, M. Liu, J. Wang, X. Su, N. Barad, J. Wang, Y.E. Sun, Q. Lin, Single-cell RNA-seq analysis revealed long-lasting adverse effects of tamoxifen on neurogenesis in prenatal and adult brains, Proc. Natl. Acad. Sci. U. S. A 117 (2020) 19578–19589.

[32] T.M. Keeley, N. Horita, L.C. Samuelson, Tamoxifen-induced gastric injury: effects of dose and method of administration, Cellular and molecular gastroenterology and hepatology 8 (2019) 365–367.

[33] X. Wu, F. Zhang, X. Xiong, C. Lu, N. Lian, Y. Lu, S. Zheng, Tetramethylpyrazine reduces inflammation in liver fibrosis and inhibits inflammatory cytokine expression in hepatic stellate cells by modulating NLRP3 inflammasome pathway, IUBMB Life 67 (2015) 312–321.

[34] M. Parola, M. Pinzani, Liver fibrosis: pathophysiology, pathogenetic targets and clinical issues, Mol Aspects Med 65 (2019) 37–55.

[35] X. Yang, L. Ma, R. Wei, T. Ye, J. Zhou, M. Wen, R. Men, R.I. Aqeilan, Y. Peng, L. Yang, Twist1-induced miR-199a-3p promotes liver fibrosis by suppressing caveolin-2 and activating TGF-β pathway, Signal Transduct. Targeted Ther. 5 (2020) 75.

[36] Y. Song, J. Wei, R. Li, R. Fu, P. Han, H. Wang, G. Zhang, S. Li, S. Chen, Z. Liu, Y. Zhao, C. Zhu, J. Zhu, S. Zhang, H. Pei, J. Cheng, J. Wu, L. Dong, G. Song, X. Shen, Q. Yao, Tyrosine kinase receptor B attenuates liver fibrosis by inhibiting TGF-β/SMAD signaling, Hepatology (Baltim., Md.) 78 (2023) 1433–1447.

[37] J. Su, S.M. Morgani, C.J. David, Q. Wang, E.E. Er, Y.-H. Huang, H. Basnet, Y. Zou, W. Shu, R.K. Soni, R.C. Hendrickson, A.-K. Hadjantonakis, J. Massagué, TGF-β orchestrates fibrogenic and developmental EMTs via the RAS effector RREB1, Nature 577 (2020) 566–571.

[38] J. Xu, M. Kitada, Y. Ogura, H. Liu, D. Koya, Dapagliflozin restores impaired autophagy and suppresses inflammation in high glucose-treated HK-2 cells, Cells 10 (2021).

[39] S.C. Sun, The non-canonical NF-κB pathway in immunity and inflammation, Nat. Rev. Immunol. 17 (2017) 545–558.

[40] M.-J. Marion, O. Hantz, D. Durantel, The HepaRG cell line: biological properties and relevance as a tool for cell biology, drug metabolism, and virology studies, Methods Mol. Biol. 640 (2010) 261–272.

[41] E. Trefts, M. Gannon, D.H. Wasserman, The liver, Curr. Biol. 27 (2017) R1147–R1151.

[42] L. Xu, A.Y. Hui, E. Albanis, M.J. Arthur, S.M. O'Byrne, W.S. Blaner, P. Mukherjee, S.L. Friedman, F.J. Eng, Human hepatic stellate cell lines, LX-1 and LX-2: new tools for analysis of hepatic fibrosis, Gut 54 (2005) 142–151.

[43] Y. Yu, L. Jiang, H. Wang, Z. Shen, Q. Cheng, P. Zhang, J. Wang, Q. Wu, X. Fang, L. Duan, S. Wang, K. Wang, P. An, T. Shao, R.T. Chung, S. Zheng, J. Min, F. Wang, Hepatic transferrin plays a role in systemic iron homeostasis and liver ferroptosis, Blood 136 (2020) 726–739.

[44] A. Wu, B. Feng, J. Yu, L. Yan, L. Che, Y. Zhuo, Y. Luo, B. Yu, D. Wu, D. Chen, Fibroblast growth factor 21 attenuates iron overload-induced liver injury and fibrosis by inhibiting ferroptosis, Redox Biol. 46 (2021) 102131.

[45] K. Du, S.H. Oh, R.K. Dutta, T. Sun, W.H. Yang, J.T. Chi, A.M. Diehl, Inhibiting xCT/SLC7A11 induces ferroptosis of myofibroblastic hepatic stellate cells but exacerbates chronic liver injury, Liver Int. 41 (2021) 2214–2227.

[46] T. Luedde, N. Kaplowitz, R.F. Schwabe, Cell death and cell death responses in liver disease: mechanisms and clinical relevance, Gastroenterology (New York, N. Y., 1943) 147 (2014).

[47] P. An, L.-L. Wei, S. Zhao, D.Y. Sverdlov, K.A. Vaid, M. Miyamoto, K. Kuramitsu, M. Lai, Y.V. Popov, Hepatocyte mitochondria-derived danger signals directly activate hepatic stellate cells and drive progression of liver fibrosis, Nat. Commun. 11 (2020) 2362.

[48] X. Liu, S. Tan, H. Liu, J. Jiang, X. Wang, L. Li, B. Wu, Hepatocyte-derived MASP1-enriched small extracellular vesicles activate HSCs to promote liver fibrosis, Hepatology (Baltim., Md.) 77 (2023) 1181–1197.

[49] Q. Zhang, Y. Qu, Q. Zhang, F. Li, B. Li, Z. Li, Y. Dong, L. Lu, X. Cai, Exosomes derived from hepatitis B virus-infected hepatocytes promote liver fibrosis via miR-222/TFRC axis, Cell Biol. Toxicol. 39 (2023) 467–481.

[50] S. Gaul, A. Leszczynska, F. Alegre, B. Kaufmann, C.D. Johnson, L.A. Adams, A. Wree, G. Damm, D. Seehofer, C.J. Calvente, D. Povero, T. Kisseleva, A. Eguchi, M.D. McGeough, H.M. Hoffman, P. Pelegrin, U. Laufs, A.E. Feldstein, Hepatocyte pyroptosis and release of inflammasome particles induce stellate cell activation and liver fibrosis, J. Hepatol. 74 (2021) 156–167.

[51] A. Zhuge, S. Li, Y. Yuan, S. Han, J. Xia, Q. Wang, S. Wang, P. Lou, B. Li, L. Li, Microbiota-induced lipid peroxidation impairs obeticholic acid-mediated antifibrotic effect towards nonalcoholic steatohepatitis in mice, Redox Biol. 59 (2023) 102582.

[52] S.J. Dixon, K.M. Lemberg, M.R. Lamprecht, R. Skouta, E.M. Zaitsev, C.E. Gleason, D.N. Patel, A.J. Bauer, A.M. Cantley, W.S. Yang, B. Morrison 3rd, B.R. Stockwell, Ferroptosis: an iron-dependent form of nonapoptotic cell death, Cell 149 (2012) 1060–1072.
[53] B.R. Stockwell, J.P. Friedmann Angeli, H. Bayir, A.I. Bush, M. Conrad, S.J. Dixon, S. Fulda, S. Gascón, S.K. Hatzios, V.E. Kagan, K. Noel, X. Jiang, A. Linkermann, M. E. Murphy, M. Overholtzer, A. Oyagi, G.C. Pagnussat, J. Park, Q. Ran, C. S. Rosenfeld, K. Salnikow, D. Tang, F.M. Torti, S.V. Torti, S. Toyokuni, K. A. Woerpel, D.D. Zhang, Ferroptosis: a regulated cell death nexus linking metabolism, Redox Biology, and Disease, Cell 171 (2017) 273–285.
[54] Y. Fu, X. Zhou, L. Wang, W. Fan, S. Gao, D. Zhang, Z. Ling, Y. Zhang, L. Ma, F. Bai, J. Chen, B. Sun, P. Liu, Salvianolic acid B attenuates liver fibrosis by targeting Ecm1 and inhibiting hepatocyte ferroptosis, Redox Biol. 69 (2024) 103029.
[55] Y. Bi, S. Liu, X. Qin, M. Abudureyimu, L. Wang, R. Zou, A. Ajoolabady, W. Zhang, H. Peng, J. Ren, Y. Zhang, FUNDC1 interacts with GPx4 to govern hepatic ferroptosis and fibrotic injury through a mitophagy-dependent manner, J. Adv. Res. 55 (2024) 45–60.
[56] X. Jiang, B.R. Stockwell, M. Conrad, Ferroptosis: mechanisms, biology and role in disease, Nat. Rev. Mol. Cell Biol. 22 (2021) 266–282.
[57] J.Y. Cao, S.J. Dixon, Mechanisms of ferroptosis, Cell. Mol. Life Sci. 73 (2016) 2195–2209.
[58] H.-F. Yan, T. Zou, Q.-Z. Tuo, S. Xu, H. Li, A.A. Belaidi, P. Lei, Ferroptosis: mechanisms and links with diseases, Signal Transduct. Targeted Ther. 6 (2021) 49.
[59] P. Koppula, Y. Zhang, L. Zhuang, B. Gan, Amino acid transporter SLC7A11/xCT at the crossroads of regulating redox homeostasis and nutrient dependency of cancer, Cancer Commun. 38 (2018) 12.
[60] X. Chen, J. Li, R. Kang, D.J. Klionsky, D. Tang, Ferroptosis: machinery and regulation, Autophagy 17 (2021) 2054–2081.
[61] Y. Zhao, H. Zhang, J.-G. Cui, J.-X. Wang, M.-S. Chen, H.-R. Wang, X.-N. Li, J.-L. Li, Ferroptosis is critical for phthalates driving the blood-testis barrier dysfunction via targeting transferrin receptor, Redox Biol. 59 (2023) 102584.
[62] X. Chen, C. Yu, R. Kang, D. Tang, Iron metabolism in ferroptosis, Front. Cell Dev. Biol. 8 (2020) 590226.
[63] T. Higashi, S.L. Friedman, Y. Hoshida, Hepatic stellate cells as key target in liver fibrosis, Adv. Drug Deliv. Rev. 121 (2017) 27–42.
[64] S.S. Cho, J.H. Yang, J.H. Lee, J.S. Baek, S.K. Ku, I.J. Cho, K.M. Kim, S.H. Ki, Ferroptosis contribute to hepatic stellate cell activation and liver fibrogenesis, Free Radic. Biol. Med. 193 (2022) 620–637.
[65] I. Mederacke, A. Filliol, S. Affo, A. Nair, C. Hernandez, Q. Sun, F. Hamberger, F. Brundu, Y. Chen, A. Ravichandra, P. Huebener, H. Anke, H. Shi, R.A. Martínez García de la Torre, J.R. Smith, N.C. Henderson, F.W.R. Vondran, C.V. Rothlin, H. Baehre, I. Tabas, P. Sancho-Bru, R.F. Schwabe, The purinergic P2Y14 receptor links hepatocyte death to hepatic stellate cell activation and fibrogenesis in the liver, Sci. Transl. Med. 14 (2022) eabe5795.
[66] Z. Xiong, P. Chen, Z. Wang, L. Yao, M. Yuan, P. Liu, M. Sun, K. Shu, Y. Jiang, Human umbilical cord-derived mesenchymal stem cells attenuate liver fibrosis by inhibiting hepatocyte ferroptosis through mitochondrial transfer, Free Radic. Biol. Med. 231 (2025) 163–177.
[67] Y. Wang, Y. Zhang, J. Xue, L. Gao, X. Li, M. Zhao, D. Zhao, X. Zhou, Ferroptosis mediates decabromodiphenyl ether-induced liver damage and inflammation, Ecotoxicol. Environ. Saf. 255 (2023) 114771.
[68] J. Tak, M.S. Joo, Y.S. Kim, H.W. Park, C.H. Lee, G.-C. Park, S. Hwang, S.G. Kim, Dual regulation of NEMO by Nrf2 and miR-125a inhibits ferroptosis and protects liver from endoplasmic reticulum stress-induced injury, Theranostics 14 (2024) 1841–1859.
[69] Y. Ge, S. Yang, T. Zhang, S. Gong, X. Wan, Y. Zhu, Y. Fang, C. Hu, F. Yang, L. Yin, Y. Pu, Z. Chen, G. Liang, Ferroptosis participated in inhaled polystyrene nanoplastics-induced liver injury and fibrosis, Sci. Total Environ. 916 (2024) 170342.
[70] S. Tsurusaki, Y. Tsuchiya, T. Koumura, M. Nakasone, T. Sakamoto, M. Matsuoka, H. Imai, C. Yuet-Yin Kok, H. Okochi, H. Nakano, A. Miyajima, M. Tanaka, Hepatic ferroptosis plays an important role as the trigger for initiating inflammation in nonalcoholic steatohepatitis, Cell Death Dis. 10 (2019) 449.
[71] Y. Kanai, B. Clémençon, A. Simonin, M. Leuenberger, M. Lochner, M. Weisstanner, M.A. Hediger, The SLC1 high-affinity glutamate and neutral amino acid transporter family, Mol Aspects Med 34 (2013) 108–120.
[72] M. Gao, P. Monian, N. Quadri, R. Ramasamy, X. Jiang, Glutaminolysis and transferrin regulate ferroptosis, Mol Cell 59 (2015) 298–308.
[73] M. Luo, L. Wu, K. Zhang, H. Wang, T. Zhang, L. Gutierrez, D. O'Connell, P. Zhang, Y. Li, T. Gao, W. Ren, Y. Yang, miR-137 regulates ferroptosis by targeting glutamine transporter SLC1A5 in melanoma, Cell Death Differ. 25 (2018) 1457–1472.
[74] A. Song, L. Wu, B.-X. Zhang, Q.-C. Yang, Y.-T. Liu, H. Li, L. Mao, D. Xiong, H.-J. Yu, Z.-J. Sun, Glutamine inhibition combined with CD47 blockade enhances radiotherapy-induced ferroptosis in head and neck squamous cell carcinoma, Cancer Lett. 588 (2024) 216727.